Quasi-elastic processes of the ^{48}Ca + ^{120}Sn system and the ^{48}Ca nuclear matter density

E. Crema,[1] M. A. G. Alvarez,[1,2] N. H. Medina,[1] L. R. Gasques,[1] J. F. P. Huiza,[3] B. Fernández,[2] Z. Abou-Haïdar,[2] P. N. de Faria,[4] P. R. S. Gomes,[4] J. Lubian,[4] and D. Verney[5]

[1]*Instituto de Física, Universidade de São Paulo, São Paulo, Brazil*

[2]*Centro Nacional de Aceleradores de la Universidad de Sevilla, CSIC, 41092 Seville, Spain*

[3]*Universidade Estadual do Sudoeste da Bahia, Bahia, Brazil*

[4]*Instituto de Fisica, Universidade Federal Fluminense, Avenida Litoranea s/n, Niterói, Rio de Janeiro, Brazil*

[5]*Institut de Physique Nucléaire, CNRS/IN2P3, Université Paris Sud, Orsay, France*

(Received 29 August 2013; published 23 October 2013)

We present the results of a high-precision quasi-elastic excitation function measurement for the ^{48}Ca + ^{120}Sn system at $\theta_{\rm LAB} = 160^{\circ}$ at near-barrier energies in steps of 1.0 MeV. The corresponding quasi-elastic barrier distribution is derived. A large-scale coupled-channel calculation was performed to investigate the role of several reaction channels in the reaction mechanism. An excellent agreement between theory and data was obtained for the barrier distribution. The first quadrupole vibrations of the ^{48}Ca and ^{120}Sn, the $2n$, and the ^{4}He transfers have a strong influence on the reaction mechanism and are responsible for the good agreement achieved. The $1n$ transfer has a minor importance in the result when compared with the $2n$ transfer, which suggests that the pairing correlation might play an important role in the $2n$-neutron transfer process. However, if the octupole vibration of the projectile is included in the coupling scheme, the agreement with the data gets worse. The comparison of the coupled-channel calculations with experimental data leads to the conclusion that the nuclear matter diffuseness of the ^{48}Ca nucleus is 0.56 fm in agreement with most of the double-magic nuclei.

DOI: 10.1103/PhysRevC.88.044616 PACS number(s): 25.70.Jj, 21.65.−f, 24.10.Eq, 21.30.Fe

I. INTRODUCTION

The double-magic ^{48}Ca nucleus has largely been used in nuclear reactions with the aim of synthesizing superheavy elements [1,2] and to study neutron transfer reactions over a large number of systems [2–6]. This is a very suitable nucleus for these kinds of investigations since it has a large number of neutrons, and so its external eight neutrons that close the rather diffuse $1f_{7/2}$ orbital seem to enhance these two kinds of processes. However, a basic nuclear property of this nucleus, its nuclear matter distribution, is yet poorly known, due to the experimental uncertainties in the neutron skin thickness [7]. Although the nuclear charge distributions of ^{40}Ca and ^{48}Ca nuclei are quite similar as supported by electron scattering, isotope shift measurements, and large-scale nuclear shell model calculations [8–10], there is a lack of experimental data on their nuclear matter distribution. Studies show that the ^{44}Ca nucleus seems to have a charge radius larger than the one of ^{40}Ca and ^{48}Ca nuclei, which makes these three calcium isotopes even more interesting to investigate experimentally [10,11]. In addition, more recently, accurate fusion excitation functions of the ^{40}Ca + ^{48}Ca [4,6], ^{48}Ca + ^{48}Ca [6,12], and ^{40}Ca + ^{40}Ca [13,14] systems have been measured to extract the fusion barrier distribution and/or to investigate the origin of the fusion hindrance that was observed at deep sub-barrier energies [15,16].

Nuclear reaction theories usually describe the nuclear interaction between projectile and target by an optical potential of Woods-Saxon form, and good fits to experimental data can be achieved by varying its six parameters. Nevertheless, despite optical potentials, which are related to the matter distributions of both interacting nuclei, it is very difficult to disentangle these potentials and to extract truthful nuclear matter distribution of each nucleus that participates in the reaction. This is because an optical potential that results from a fit procedure has six free parameters and, therefore, has large ambiguities. In addition, the real and imaginary terms of the optical potential are not independent of each other since they are related by a dispersion relation [17]. So, to avoid these limitations inherent to the analysis based on optical potentials, recently, we have developed a method that allows the derivation of the nuclear matter diffuseness from heavy-ion reaction data [18,19]. In the present paper, we apply the same method to the ^{48}Ca nucleus.

As is well known, quasi-elastic barrier distributions (QEBDs), measured at backward angles and energies near the Coulomb barrier, are very sensitive to the nuclear structure of the interacting nuclei [20,21]. For most of the heavy-ion collisions, QE scattering means the sum of elastic scattering, inelastic excitations of low-lying states, and few-nucleon transfers to low-lying states of the residual nuclei. The QEBD is calculated by the first derivative, with respect to energy, of the ratio of the quasi-elastic differential cross section to the corresponding Rutherford differential cross section $d(\sigma_{\rm qel}/\sigma_{\rm Ruth})/dE$ [20,21]. As data are taken at backward angles and low relative velocities between the interacting nuclei, this process is dominated by quantum tunneling, and consequently, it is very sensitive to the potential details. Besides, the use of a derivative of experimental data to obtain the QEBD may evidence small reaction effects hidden in the smoothness of QE excitation functions, which makes this method even more sensitive to the potential shape.

When heavy nuclei are involved in the reaction, even at sub-barrier energies, besides the QE reactions, other processes can play a significant role in the reaction mechanism, such as deep inelastic collisions (DICs) [22–24], multinucleon transfers [25–28], and inelastic excitations of high-lying states

[29]. In addition, for weakly bound systems, breakup can also be a relevant part of QE events [30]. Rehm *et al.* [23] investigated the ^{48}Ti + ^{208}Pb system, and they have shown that, at forward angles and well above the Coulomb barrier, the transition from QE scattering to DIC evolves gradually and it is experimentally difficult to separate them because they are superposed to each other in the energy spectra. Besides, Mitsuoka *et al.* [24] measured the QE excitation function at $\theta_{\mathrm{LAB}} = 172^{\circ}$ at energies close to the Coulomb barrier for the same system, and the results have shown that the deep inelastic processes are still present even at incident energies below the barrier. Other interesting works are the measurements of backscattering in the lighter ^{16}O + ^{208}Pb system at sub-barrier energies with the aim of investigating the diffuseness of Woods-Saxon potentials [26–28]. In these studies, apart from the QE events, there also is one superposing group of high-dissipative events with Q values up to -23 MeV, identified as produced mainly from complex cluster transfer reactions [27]. Recently, it was suggested [29] that those dissipative events may also be due to the excitation of high-energy noncollective states. However, for most systems, the process which produces high-dissipative collisions in reactions where there is not enough energy in the entrance channel is still under debate. Nevertheless, independent of the possible reaction mechanisms which may produce these highly dissipative projectilelike fragments (PLFs), a qualitative analysis of all experimental energy spectra cited above shows that the importance of these events and their corresponding dissipation increase with the mass symmetry and mass of the system. In the present paper, to contribute to this field, we have measured a high-precision excitation function at $\theta_{\mathrm{LAB}} = 160^{\circ}$ for the ^{48}Ca + ^{120}Sn system, which is more symmetrical than the others discussed above.

With concern for the derivation of the nuclear matter and charge densities of the interacting nuclei from backward QE measurements, a crucial point is the choice of a reliable interaction bare potential, which is directly related to those quantities. In previous papers [18,19] and in the present one, we used the energy-independent part of the São Paulo potential (SPP) that has been very successful for explaining a wide range of reaction processes in more than 100 light and heavy systems [31]. The SPP is a double-folding potential calculated with the two-parameter-Fermi shape for both the nuclear and the charge densities. In this way, it is possible to search for the correct density parameter values by varying them and by fitting data with theoretical coupled-channel calculations. From this method, one might have four parameters for the target and four parameters for the projectile. In previous papers, including the present one, we reduce the number of free parameters to one, as we explain in the following. Experimental and theoretical values of the average charge and matter radii of a large number of nuclei plotted against $Z^{1/3}$ and $A^{1/3}$, respectively, have shown linear systematic behaviors with very little dispersion around the average values of $R_{\mathrm{CH}} = (1.76Z^{1/3} - 0.96)$ and $R_{\mathrm{MATT}} = (1.31A^{1/3} - 0.84)$ fm [31]. However, this is not the case for the diffuseness parameters that show large dispersion around the average values of $a_{\mathrm{CH}} = 0.53$ and $a_{\mathrm{MATT}} = 0.56$ fm, which reflect the shell and structure effects of the different nuclei. So, in the present paper, to reduce the number of free density parameters in the fit procedure, we have used the ^{120}Sn nucleus as the target for which the diffuseness is well described by the average values of the systematic. So, only the diffuseness parameters of the ^{48}Ca projectile are unknown and will be derived in the present paper.

Another very important point of our method is that we do not use any imaginary potential at the nuclear surface region in our calculations to avoid double counting of the reaction channels, which are directly included in the coupling scheme. Instead, we perform very large coupled-channel calculations by including as much reaction channels as possible in the coupling matrix, which turns out to make the use of an imaginary potential unnecessary. It is very important to mention that we are not interested in getting a perfect fit of the QE excitation function over the entire energy range investigated but rather a good fit around the barrier where the concept of QE barrier distribution is meaningful.

In Sec. II, we describe the experiment, present the results, and deduce the quasi-elastic barrier distribution of the ^{48}Ca + ^{120}Sn system. In Sec. III, we describe the large-scale coupled-channel calculations. In Sec. IV, we deduce the nuclear matter and charge diffuseness of the ^{48}Ca nucleus and discuss the results. Finally, we present the conclusions in Sec. V.

II. EXPERIMENTAL DETAILS AND RESULTS

The experiment was performed at the Tandem/ALTO facility of the Institute of Nuclear Physics, Orsay, France. Beams of ^{48}Ca were delivered at energies that range from 152 to 175 MeV in steps of 1.0 MeV. The nominal Coulomb barrier is around 161 MeV. The self-supporting ^{120}Sn target was enriched to 98.80% and had a thickness of 135 μg/cm^2. As the beam intensities were less than 5 nA and the QE barrier distribution method demands a large number of counts at a backward direction, the solid angle of the detector system was improved by mounting out-of-plane four large area silicon detectors (300 mm^2) at $\theta_{\mathrm{LAB}} = 160^{\circ}$, each of them covering an angular range of 3.2°. Data normalization and beam monitoring were provided by two silicon detectors placed at $\pm 30^{\circ}$.

Figure 1 presents two typical PLF energy spectra at $\theta_{\mathrm{LAB}} = 160^{\circ}$ (converted into their correspondent Q spectra) for the ^{48}Ca + ^{120}Sn system, where $Q = 0$ MeV corresponds to the elastic scattering. The top panel (a) shows the spectrum taken at a bombarding energy of 154 MeV, which is 7.0 MeV below the Coulomb barrier (V_{B}), i.e., $E/V_{\mathrm{B}} = 0.96$, approximately. This spectrum is similar to those measured in Ref. [24] at $\theta_{\mathrm{LAB}} = 172^{\circ}$ for the ^{48}Ti, ^{54}Cr, ^{56}Fe, ^{64}Ni, and ^{70}Zn + ^{208}Pb systems at equivalent E/V_{B} values. The spectrum in Fig. 1(a) presents three overlapping groups of events. One, with most of the events placed around $Q = 0$ MeV, represents the elastic scattering and the low-lying excitations of the target and the projectile, which are not resolved from each other. A second group of events is located around $Q = -5$ MeV and mainly is produced by two quadrupole and one octupole excitations of the ^{48}Ca: (2^+,3.83 MeV), (3^-,4.50 MeV), and (2^+,6.80 MeV), which are unresolved.

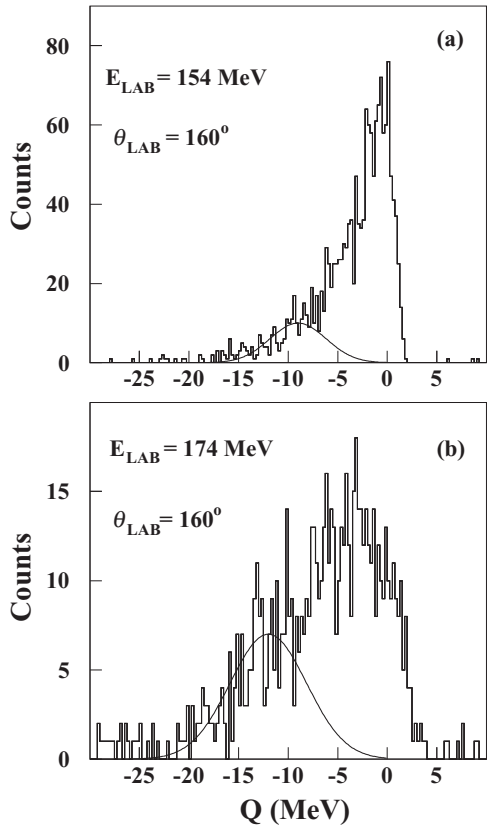

FIG. 1. Measured Q-value spectra at $\theta_{\rm LAB} = 160^{\circ}$ for the ^{48}Ca + ^{120}Sn system at bombarding energies of (a) 154 MeV and (b) 174 MeV. The solid curves serve to guide the eye and are discussed in the text.

As will be discussed later, the calculated cross sections of these three inelastic excitations at this energy are large enough to explain the events of this second group. Finally, the last group of events is centered at $Q = -9$ MeV and extends up to $Q = -20$ MeV, which is represented in Fig. 1(a) by a Gaussian curve used as a guide for the eye. To get an insight into the origin of these events, we have calculated the inelastic cross sections of states of the projectile and target with excitation energies up to 10 MeV and their mutual excitations. The calculated inelastic cross sections were too small to explain the highly dissipative collisions that populate this energy region of the spectrum, although inelastic excitations can produce some of those events. In addition, according to the calculations to be presented in the next section, the direct transfer of a few nucleons cannot explain those dissipative events for the same reason. Their transfer cross sections have been calculated by a large-scale coupled-channel calculation, which includes the $1n$-, $2n$-, $2p$-, ^{3}He-, and ^{4}He-transfer processes between high-lying states of ^{48}Ca and ^{120}Sn. So, as was performed in Ref. [24], we will call these highly dissipative events of our spectra deep inelastic processes, which include very high inelastic excitations and multinucleon transfer processes. Irrespective to their origins, these events will be excluded from the "conventional" QE events that we are interested in. Later in this paper, we will show that the resulting barrier distribution is not very affected by these events. A perfect identification of their origins would demand another dedicated experiment as the one performed in Ref. [27] with small collimators and good energy resolution, which is incompatible with a barrier distribution measurement that uses a low intensity beam, as was performed in the present paper. The most dissipative PLFs in the spectrum of Fig 1(a) have an average energy dissipation of about 9 MeV, which is smaller and compatible with the results of Ref. [24], which show that, for equivalent $E/V_{\rm B}$ values, the average energy dissipation of the DIC in heavier systems evolves from $Q = -60$ MeV for ^{70}Zn + ^{208}Pb up to $Q = -20$ MeV for ^{48}Ti + ^{208}Pb, approximately.

Figure 1(b) shows that, when the bombarding energy increases to 174 MeV, i.e., about 14 MeV above the Coulomb barrier ($E/V_{\rm B} = 1.08$), the general characteristics of the spectrum remain the same, but the relative intensity of the three groups changes significantly. The relation between the elastic scattering cross section and the inelastic scattering plus the transfer reaction cross sections decreases. This behavior is confirmed by our theoretical calculations which will be presented in the next section. Besides, as expected, the most dissipative collisions become more important than at lower energies, and its average Q value is now around -12 MeV.

To obtain the QE cross section, the QE events must be separated from the more dissipative ones. Some procedures to perform this separation are discussed in Refs. [23,24]. One of them is to use a low-energy cutoff defined by a Q value that only retains the elastic scattering, inelastic scattering, and few-nucleon transfers to low-lying energy states, that is, the conventional QE events. The value of this energy cutoff is suggested by the experimental spectra themselves [23,24]. In our experiment, the first minimum of the spectrum, shown in Fig. 1(a), indicates that a reasonable upper limit for the QE events is around $Q = -7$ MeV. Alternatively, one could separate the two kinds of events by fitting the low-energy tail of the spectra with a Gaussian function as shown in Fig. 1. This method is based on the hypothesis that the DIC component is composed of fully damped projectilelike nuclei which have Gaussian distributions of mass and total kinetic energy. This hypothesis is confirmed by Monte Carlo reaction simulations [24]. We used both methods, and they gave similar results within the experimental uncertainties. A variation of ± 1.0 MeV in the energy cutoff produces an uncertainty in the QE events from 2% (lowest energy) to 9% (highest energy), approximately. By taking this cutoff uncertainty into account, the overall statistical uncertainty in the QE excitation function ranges from 3.6% to 12.6%.

The solid-circle symbols in Fig. 2 are the experimental results of (a) the QE excitation function at $\theta_{\rm LAB} = 160^{\circ}$ for the ^{48}Ca + ^{120}Sn system and (b) the corresponding QE barrier distribution derived by using the point difference method with energy steps of $\Delta E_{\rm LAB} = 2$ MeV. The energies were corrected by the centrifugal energy and energy loss in the target. Figure 2 also shows the excitation function and the corresponding barrier distribution of the inclusive events without the extraction of the DIC contribution (star symbols). Both excitation functions (divided by the Rutherford cross section) were normalized to unity at the lowest energies. The excitation functions are similar, except at energies above $E_{\rm CM} =$ 120 MeV where the differences start to become significant in

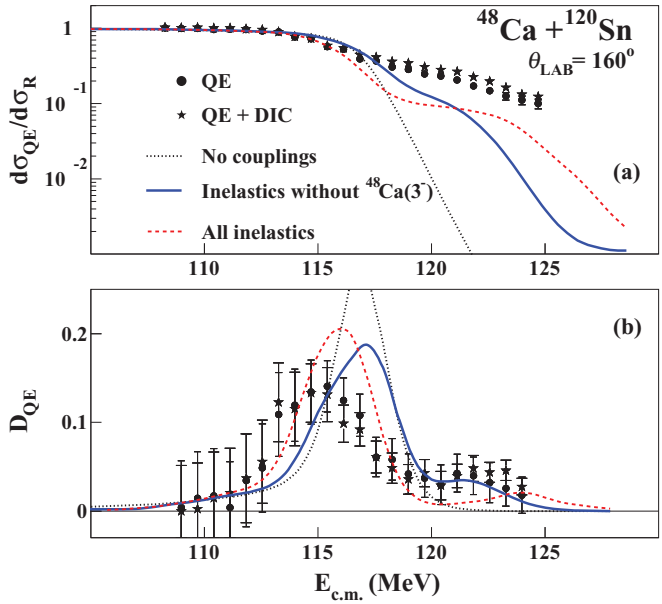

FIG. 2. (Color online) (a) Measured quasi-elastic excitation function (solid circles) taken at $\theta_{LAB} = 160^\circ$ for the ^{48}Ca + ^{120}Sn system and (b) the corresponding deduced experimental quasi-elastic barrier distribution for the same system. For comparison, the inclusive data are also plotted (star symbols). The curves are discussed in the text.

the excitation function, but they are negligible in the barrier distributions shown in Fig. 2(b). A qualitative analysis of Fig. 2(b) shows that the QE barrier distribution has a wider main peak (Coulomb barrier) centered at $E_{CM} = 115$ MeV and a secondary peak at $E_{CM} = 121$ MeV, approximately. The other curves of Fig. 2 will be explained in the next section.

III. COUPLED-CHANNEL CALCULATIONS

As discussed in Sec. I, in our coupled-channel calculations, we use a double-folding potential to simulate the nuclear interaction between projectile and target. In this section, all potentials are constructed with the average values of the density parameters obtained by a large systematic study [31]. Within this approach, calculations have no free parameters, and their results are to be directly compared with the experimental data. Another important point to mention again, which concerns our procedure, is the absence of any imaginary potential at the interaction region surface. Since a very large number of reaction channels is included in the coupling matrix, the surface imaginary potential is unnecessary, at least, at energies close to the Coulomb barrier, otherwise, it would lead to double counting the effects of the reaction channels included in the calculations. On the other hand, to take the fusion process (which is not explicitly included in the coupling matrix) into account, an inner imaginary potential of Woods-Saxon form is used: $V_{IM} = 80$ MeV, $r_{IM} = 0.9$, and $a_{IM} = 0.2$ fm. The coupled-channel calculations were performed by using the code FRESCO [32].

TABLE I. Excited states included in the coupled-channel calculations.

Nucleus	I^π	E (MeV)
^{48}Ca	0^+	0
^{48}Ca	2^+	3.83
^{48}Ca	0^+	4.28
^{48}Ca	4^+	4.50
^{48}Ca	3^-	4.51
^{48}Ca	2^+	6.81
^{48}Ca	2^+	8.88
^{120}Sn	0^+	0
^{120}Sn	2^+	1.17
^{120}Sn	0^+	1.87
^{120}Sn	2^+	2.10
^{120}Sn	4^+	2.19

A. Coupling of inelastic excitations

Table I shows the excited states of projectile and target nuclei that were considered in the couplings. Actually, we included all excited states for which there was experimental information about their transition probabilities in Ref. [33]. Figure 2 shows the results of the calculations compared to (a) the experimental QE excitation function and (b) the corresponding QE barrier distribution. The theoretical QE barrier distribution was calculated with the same procedure used to derive the experimental barrier distribution. The thin-dotted curve in Fig. 2 is the result of a calculation with no coupling and represents the effect of the bare real nuclear potential. One can see that the uncoupled Coulomb barrier is located at $E_{c.m.} = 117$ MeV, approximately. The blue-solid curves represent the coupling of all considered excitation states of the projectile and the target, except the octupole vibration (3^-) of ^{48}Ca.

These inelastic excitations have a strong influence on the reaction mechanism and produce a large enhancement of the QE excitation function at energies above the Coulomb barrier. Among the inelastic states included in the calculation, the most important are, as expected, the first quadrupole vibrations of ^{48}Ca and ^{120}Sn. By considering how the theoretical curves evolve when the inelastic excitations are included in the coupling matrix, we concluded that, if more channels were included in the calculations, it could be possible to improve the agreement with the high-energy part of the experimental QE excitation function [see Fig. 2(a)]. However, there is a lack of data on the experimental transition probabilities for the other transitions of ^{48}Ca and ^{120}Sn, not included in our calculations.

The blue-solid curve in Fig. 2(b) shows the strong effect of the inelastic excitations on the QE barrier distribution when compared with the uncoupled barrier. The Coulomb barrier is wider, and the small barrier at 121 MeV is now nicely predicted. It is interesting to observe that this small barrier is above the Coulomb barrier by an energy value equal to the sum of the excitation energies of the first 2^+ states of ^{48}Ca and ^{120}Sn, approximately. This means that this barrier should be produced by these two channels. The red-dashed curves in Fig. 2 present the strong effect of coupling the octupole vibration of ^{48}Ca

TABLE II. $Q_{g.s.}$ values of transfer reactions in the ^{48}Ca + ^{120}Sn system.

Transfer	$Q_{g.s.}$ (MeV)
1n stripping	− 3.782
2n stripping	− 2.240
^{4}He pickup	+ 2.865
^{3}He pickup	+ 0.827
2p pickup	+ 2.809

(3$^-$,4.50 MeV). It destroys the reasonable agreement with the data already obtained by the other inelastic excitations. Figure 2(b) shows that the entire barrier distribution is shifted down in energy by about 1.0 MeV, the shape of the main peak of the distribution is almost unchanged, and the agreement with the data is worse. This behavior is found in almost all coupled-channel calculations that involve one (or more) high-lying 3$^-$ states. The most studied one is the state of ^{16}O (3$^-$,6.13 MeV), which presents almost the same behavior as the one of ^{48}Ca (3$^-$,4.50 MeV) [34,35]. Actually, the solution of coupled equations that include any state with excitation energy higher than the barrier curvature produces an adiabatic renormalization of the bare potential. Usually, as bare potentials are obtained from fits to experimental data, which already carry the octupole effect in them, these states must be excluded from the calculation to avoid double counting. Or, as was performed in Ref. [29], if 3$^-$ states are explicitly included in the calculation and the bare potential comes from data analysis, the potential must be changed to compensate the adiabatic renormalization produced by the octupole vibration. In this paper, since the bare potential used is a double-folding potential, deduced from first principles, it is free from this kind of contamination, and all reaction channels can explicitly be included in the calculation. However, in the present calculations, the ^{48}Ca (3$^-$) state does not seem to be very important in the reaction mechanism.

B. Coupling of transfer channels

For the coupling of transfer channels, all calculations were performed by using the coupled reaction channel method, which uses the exact finite-range prior approximation. For the transitions of one nucleon, pure single-particle states were used. In the case of multinucleon transfer, the cluster model was used. The wave function of the cluster was obtained by a superposition of the single-particle wave function to form a cluster with spin zero (except for the ^{3}He transfer where its ground-state spin was used). As there is no available spectroscopic amplitude information for all included overlaps, we assumed the value of 1.0. This is a reasonable assumption as far as we are considering pure single-particle state transition. We have tested all positive Q-value channel effects on the QE barrier distribution and some negative Q-value channels. As we are dealing with near-barrier reactions and the high-dissipative events were excluded from the data, the very negative Q-value channels ($Q_{g.s.} < -5$ MeV) were not included in the calculations. For the transfer form factors, Woods-Saxon potentials were assumed. For the reduced radii and diffuseness, standard values of 1.2 and 0.6 fm were assumed. The depths of the potential were varied automatically to fit the experimental binding energies.

TABLE III. Overlaps between states of the projectile and the target considered in coupled-channel calculations.

^{120}Sn(^{48}Ca,^{47}Ca)^{121}Sn	^{120}Sn(^{48}Ca,^{46}Ca)^{122}Sn	^{120}Sn(^{48}Ca,^{52}Ti)^{116}Cd
$\langle^{48}$Ca(0$^+$, g.s.)$\vert^{47}$Ca(7/2$^-$, g.s.)$\rangle$	$\langle^{48}$Ca(0$^+$, g.s.)$\vert^{46}$Ca(0$^+$, g.s.)$\rangle$	$\langle^{48}$Ca(0$^+$, g.s.)$\vert^{52}$Ti(0$^+$, g.s.)$\rangle$
$\langle^{48}$Ca(0$^+$, g.s.)$\vert^{47}$Ca(3/2$^-$, 2.013)$\rangle$	$\langle^{48}$Ca(2$^+$, 3.832)$\vert^{46}$Ca(0$^+$, g.s.)$\rangle$	$\langle^{120}$Sn(0$^+$, g.s.)$\vert^{116}$Cd(0$^+$, g.s.)$\rangle$
$\langle^{48}$Ca(0$^+$, g.s.)$\vert^{47}$Ca(3/2$^+$, 2.578)$\rangle$	$\langle^{48}$Ca(0$^+$, 4.283)$\vert^{46}$Ca(0$^+$, g.s.)$\rangle$	$\langle^{120}$Sn(0$^+$, g.s.)$\vert^{116}$Cd(2$^+$, 0.513)$\rangle$
$\langle^{48}$Ca(0$^+$, g.s.)$\vert^{47}$Ca(1/2$^+$, 2.559)$\rangle$	$\langle^{48}$Ca(0$^+$, g.s.)$\vert^{46}$Ca(2$^+$, 1.346)$\rangle$	$\langle^{120}$Sn(0$^+$, g.s.)$\vert^{116}$Cd(4$^+$, 1.219)$\rangle$
$\langle^{48}$Ca(0$^+$, g.s.)$\vert^{47}$Ca(7/2$^-$, 3.425)$\rangle$	$\langle^{48}$Ca(0$^+$, g.s.)$\vert^{46}$Ca(0$^+$, 2.423)$\rangle$	^{120}Sn(^{48}Ca,^{51}Ti)^{117}Cd
$\langle^{120}$Sn(0$^+$, g.s.)$\vert^{121}$Sn(3/2$^+$, g.s.)$\rangle$	$\langle^{48}$Ca(0$^+$, g.s.)$\vert^{46}$Ca(4$^+$, 2.575)$\rangle$	$\langle^{48}$Ca(0$^+$, g.s.)$\vert^{51}$Ti(3/2$^-$, g.s.)$\rangle$
$\langle^{120}$Sn(0$^+$, g.s.)$\vert^{121}$Sn(11/2$^-$, 0.006)$\rangle$	$\langle^{120}$Sn(0$^+$, g.s.)$\vert^{122}$Sn(0$^+$, g.s.)$\rangle$	$\langle^{48}$Ca(0$^+$, g.s.)^{51}Ti(1/2$^-$, 1.166)$\rangle$
$\langle^{120}$Sn(0$^+$, g.s.)$\vert^{121}$Sn(1/2$^+$, 0.060)$\rangle$	$\langle^{120}$Sn(0$^+$, g.s.)$\vert^{122}$Sn(2$^+$, 0.513)$\rangle$	$\langle^{48}$Ca(0$^+$, g.s.)$\vert^{51}$Ti(7/2$^-$, 1.437)$\rangle$
$\langle^{120}$Sn(0$^+$, g.s.)$\vert^{121}$Sn(5/2$^+$, 0.869)$\rangle$	$\langle^{120}$Sn(0$^+$, g.s.)$\vert^{122}$Sn(4$^+$, 1.219)$\rangle$	$\langle^{48}$Ca(0$^+$, g.s.)$\vert^{51}$Ti(5/2$^-$, 2.144)$\rangle$
$\langle^{120}$Sn(0$^+$, g.s.)$\vert^{121}$Sn(5/2$^+$, 0.908)$\rangle$	$\langle^{120}$Sn(0$^+$, g.s.)$\vert^{122}$Sn(4$^+$, 2.331)$\rangle$	$\langle^{48}$Ca(0$^+$, g.s.)$\vert^{51}$Ti(3/2$^-$, 2.198)$\rangle$
$\langle^{120}$Sn(0$^+$, g.s.)$\vert^{121}$Sn(7/2$^+$, 0.925)$\rangle$	$\langle^{120}$Sn(0$^+$, g.s.)$\vert^{122}$Sn(2$^+$, 2.415)$\rangle$	$\langle^{120}$Sn(0$^+$, g.s.)$\vert^{117}$Cd(1/2$^+$, g.s.)$\rangle$
$\langle^{120}$Sn(0$^+$, g.s.)$\vert^{121}$Sn(7/2$^-$, 0.949)$\rangle$	$\langle^{120}$Sn(0$^+$, g.s.)$\vert^{122}$Sn(6$^+$, 2.555)$\rangle$	$\langle^{120}$Sn(0$^+$, g.s.)$\vert^{117}$Cd(3/2$^+$, 0.13)$\rangle$
$\langle^{120}$Sn(0$^+$, g.s.)$\vert^{121}$Sn(3/2$^+$, 1.101)$\rangle$	$\langle^{120}$Sn(0$^+$, g.s.)$\vert^{122}$Sn(2$^+$, 2.775)$\rangle$	$\langle^{120}$Sn(0$^+$, g.s.)$\vert^{117}$Cd(5/2$^+$, 0.06)$\rangle$
$\langle^{120}$Sn(0$^+$, g.s.)$\vert^{121}$Sn(5/2$^+$, 1.121)$\rangle$	$\langle^{120}$Sn(0$^+$, g.s.)$\vert^{122}$Sn(4$^+$, 2.959)$\rangle$	$\langle^{120}$Sn(0$^+$, g.s.)$\vert^{117}$Cd(5/2$^+$, 0.69)$\rangle$
	$\langle^{120}$Sn(0$^+$, g.s.)$\vert^{122}$Sn(4$^+$, 2.973)$\rangle$	^{120}Sn(^{48}Ca,^{50}Ti)^{118}Cd
	$\langle^{120}$Sn(0$^+$, g.s.)$\vert^{122}$Sn(4$^+$, 3.082)$\rangle$	$\langle^{48}$Ca(0$^+$, g.s.)$\vert^{50}$Ti(0$^+$, g.s.)$\rangle$
	$\langle^{120}$Sn(0$^+$, g.s.)$\vert^{122}$Sn(2$^+$, 3.129)$\rangle$	$\langle^{48}$Ca(0$^+$, g.s.)$\vert^{50}$Ti(2$^+$, 1.554)$\rangle$
		$\langle^{120}$Sn(0$^+$, g.s.)$\vert^{118}$Cd(0$^+$, g.s.)$\rangle$
		$\langle^{120}$Sn(0$^+$, g.s.)$\vert^{118}$Cd(2$^+$, 0.488)$\rangle$
		$\langle^{120}$Sn(0$^+$, g.s.)$\vert^{118}$Cd(4$^+$, 1.165)$\rangle$

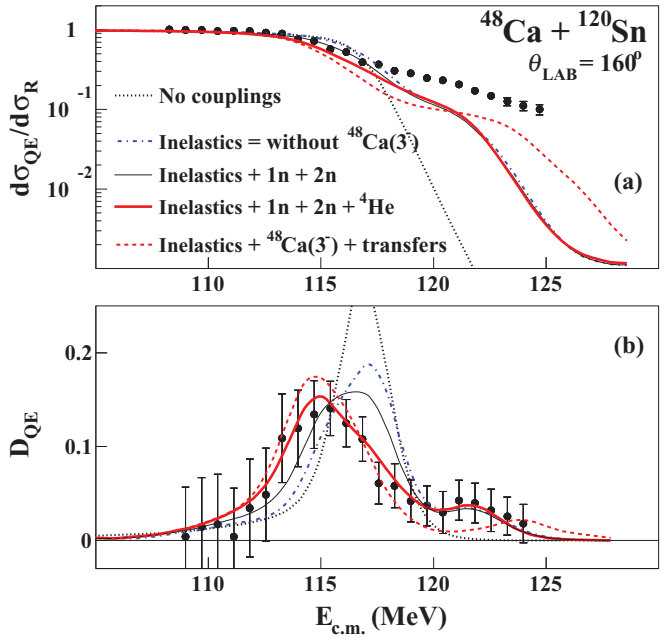

FIG. 3. (Color online) Results of the coupled-channel calculations compared to experimental data taken at $\theta_{LAB} = 160^\circ$ for the ^{48}Ca + ^{120}Sn system. (a) Quasi-elastic excitation function and (b) deduced experimental quasi-elastic barrier distribution. The curves are discussed in the text.

Tables II and III present the $Q_{g.s.}$ values of the transfer processes and the overlaps between the states that were considered in this paper. We have included the transfer channels one by one in the calculation to investigate the effect of each one. The state ^{48}Ca (3$^-$) was coupled only at the last step to isolate its strong effect. Figure 3 presents the results of the channels that had more influence on the QE excitation function and barrier distribution. The dotted curves in Fig. 3 are the results of the calculations without any couplings. The blue-dashed-dotted curves are the results of the coupling of the inelastic channels [without ^{48}Ca (3$^-$)] discussed in the previous section and are shown here as a reference result. The black-thin-solid curves show the results when the 1n- and 2n-stripping reactions are included in the calculations by considering all excited states presented in Table III. Despite being presented together, these results have a minor contribution from the 1n transfer. This is an interesting result that could be due to a strong pairing correlation between the two neutrons transferred to the target like the strong pairing correlation recently reported in two-proton transfer reactions [27]. Compared to the effects of the inelastic channels, the QE excitation function is affected by the 1n- and 2n-transfer channels only at energies between 112 and 118 MeV. On the other hand, Fig. 3(b) shows that the QE barrier distribution changes significantly with the inclusion of these channels in the calculation. The main barrier is flattened, and a small shift down in energy is observed, whereas, above 120 MeV, there is no effect at all.

The red-solid curves in Fig. 3 are the results of adding the ^{4}He transfer to the previous coupled calculation. Although the QE excitation function presents only a small effect of this channel, the QE barrier distribution shows that it actually has a strong influence on the reaction mechanism of this system, only observed in the barrier distribution. The main barrier is slightly sharpened and shifted down in energy. As its $Q_{g.s.}$ value is large and positive, the ^{4}He transfer does not influence the high-energy part of the barrier distribution. Figure 3(b) shows that very nice agreement with the experimental QE barrier distribution over its entire energy range is obtained with the coupling of the channels already considered. The inclusion of the ^{3}He and 2p transfers has a minor effect on both the QE excitation function and the barrier distribution. Finally, all transfer channels shown in Table III were coupled together with all inelastic channels discussed above, which include ^{48}Ca (3$^-$). The result of the coupling of these 61 channels is represented by the red-dashed curve in Fig. 3. The differences observed with respect to the previous calculation are largely due to the ^{48}Ca (3$^-$) state. With the inclusion of this channel, the agreement with the experimental QE excitation function is improved only at the highest energies, whereas, between 114 and 122 MeV, the agreement gets worse. Figure 3(b) shows that inclusion of the ^{48}Ca (3$^-$) state in the coupling matrix destroys the excellent agreement already obtained between the theoretical QE barrier distribution and the experimental barrier, which indicates that the octupole vibration of ^{48}Ca probably is not very excited during the collisions, despite its large theoretical cross section. It is also interesting to observe that the inclusion of the ^{48}Ca (3$^-$) state in the last step of the calculation shifted down the entire distribution by only 0.2 MeV, whereas, the shift observed in Fig. 2 was 1.0 MeV. This indicates that care must be taken with concern for the conclusions when only a few channels are coupled in the calculation. On the other hand, the inclusion of several channels in the coupling matrix may be a problem for some of the available coupled-channel codes.

IV. THE ^{48}Ca MATTER DIFFUSENESS

One of the aims of the present paper was the search for a bare double-folding potential that reproduces the experimental barrier distribution. As discussed in Sec. I, in our search procedure, only the charge- and matter-diffuseness values of ^{48}Ca and ^{120}Sn might be parameters to be changed. In order to investigate the ^{120}Sn nucleus, we have used our method to analyze the quasi-elastic barrier distribution of the ^{16}O + ^{120}Sn system measured by Sinha *et al.* [36]. The ^{16}O diffuseness parameters had already been determined [18], and their values were found as those of the systematics of the SPP. Then, the diffuseness parameters of the ^{120}Sn nucleus were isolated as the only free parameters to be determined. The results showed that the position and shape of the barrier distribution for this system are well described by the average values of the systematics for both charge and matter nuclear parameters: $a_{CH} = 0.53$ and $a_{MATT} = 0.56$ fm.

Then, for the ^{48}Ca + ^{120}Sn system, only the ^{48}Ca diffuseness values were left to be determined. The starting point of our calculations was the average values of $a_{CH} = 0.53$ and $a_{MATT} = 0.56$ fm for ^{48}Ca. As we have shown in the previous section, the first calculations gave such excellent results that

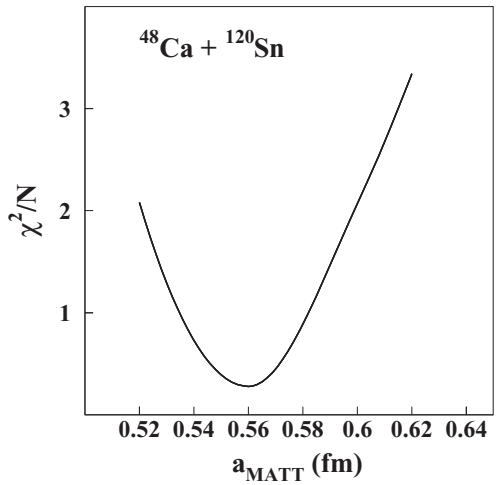

FIG. 4. Results of the χ^2 analysis of the QE barrier distribution for the ^{48}Ca + ^{120}Sn system. The average χ^2 per data point is plotted against the nuclear matter diffuseness of the projectile.

we concluded that those values should be close to the correct ones for ^{48}Ca. In the next step, we kept the charge diffuseness constant ($a_{CH} = 0.53$ fm) and changed the matter diffuseness around the value of 0.56 fm to find its best value through a χ^2 analysis of the QE barrier distribution. The result of this procedure is shown in Fig. 4 where the average χ^2 per data point is plotted against a_{MATT}. As can be seem in Fig. 4, this kind of calculation is very sensitive to the diffuseness parameter, and a pronounced valley with a minimum around 0.56 fm is observed. Then, we can conclude that, according our method and the systematic values of Ref. [31], the matter distribution of ^{48}Ca has a diffuseness of 0.56 fm, which is the value of most double-magic nuclei.

Recently, fusion data of ^{48}Ca + ^{48}Ca [12] have been analyzed with an interesting theoretical approach that also uses double-folding potentials [37]. In that paper, the ion-ion potential was calculated by using a nuclear density parametrization somehow different from the Fermi function density used in the SPP, and a repulsive core potential was added to generate the shallow potentials that are necessary to reproduce the fusion data at deep sub-barrier energies. All these differences between the potentials used in Ref. [37] and the potentials used in the present paper make any precise and quantitative comparison of their results difficult. However, it is interesting to mention that the best fit to the fusion data was obtained by using a nuclear diffuseness equal to 0.54 fm in the calculation of the direct and exchange parts of the double-folding potential. Very recently, the same theoretical approach of Ref. [37] was employed in the analysis of the ^{40}Ca + ^{40}Ca fusion data, and the best fit was attained with a nuclear diffuseness equal to 0.56 fm [14]. All these results show that ^{40}Ca and ^{48}Ca have similar matter diffuseness. On the other hand, isotopic shift measurements and theoretical predictions show that ^{44}Ca has a charge radius larger than the other calcium isotopes [10,11]. We plan a similar paper in the near future that uses ^{44}Ca as a projectile to investigate this very interesting nucleus.

V. CONCLUSIONS

We have measured a high-precision quasi-elastic excitation function for the ^{48}Ca + ^{120}Sn system at $\theta_{LAB} = 160^\circ$ and beam energies that range from 152 to 175 MeV in steps of 1.0 MeV. The corresponding quasi-elastic barrier distribution was derived by using the conventional point-difference method. Large-scale coupled-channel calculations were performed to investigate the role of several reaction channels in the reaction mechanism of this system. Excellent agreement between theory and data was obtained for the barrier distribution if the octupole vibration of the projectile is kept out of the coupling scheme. The first quadrupole vibrations of ^{48}Ca and ^{120}Sn, the $2n$ transfer, and ^{4}He transfer, have strong influences on the reaction mechanism and are responsible for the good agreement obtained. The $1n$ transfer has a minor importance in the result when compared with the $2n$ transfer, which suggests that the pairing correlation may play an important role in the $2n$-neutron transfer process. Finally, the comparison of the coupled-channel calculation with experimental data supports that the nuclear matter diffuseness of the ^{48}Ca nucleus is 0.56 fm as most of the double-magic nuclei. We have shown that the use of quasi-elastic barrier distributions is a powerful and very sensitive tool to derive properties of the structure of nuclei in addition to the well-established importance of this quantity to the investigation of reaction mechanisms.

ACKNOWLEDGMENTS

The authors acknowledge the financial support of Fundação de Amparo à Pesquisa do Estado de São Paulo (FAPESP-Brazil), Fundação de Amparo à Pesquisa do Estado do Rio de Janeiro (FAPERJ-Brazil), Conselho Nacional de Desenvolvimento Científico e Tecnológico (CNPq-Brazil), The Pronex (Brazil), and the European Community FP7—Capacities-Integrated Infrastructure Initiative—Contract No. ENSAR 262010. The authors thank the TANDEM-ALTO Laboratory for its hospitality and, particularly, its crew for the technical support and beam operation.

[1] Y. T. Oganessian *et al.*, Phys. Rev. Lett. **109**, 162501 (2012).
[2] Y. T. Oganessian *et al.*, Phys. Rev. C **87**, 034605 (2013).
[3] G. Montagnoli *et al.*, Phys. Rev. C **87**, 014611 (2013).
[4] C. L. Jiang *et al.*, Phys. Rev. C **82**, 041601(R) (2010).
[5] A. M. Stefanini *et al.*, Phys. Rev. C **73**, 034606 (2006).
[6] M. Trotta, A. M. Stefanini, L. Corradi, A. Gadea, F. Scarlassara, S. Beghini, and G. Montagnoli, Phys. Rev. C **65**, 011601 (2001).
[7] C. J. Horowitz, S. J. Pollock, P. A. Souder, and R. Michaels, Phys. Rev. C **63**, 025501 (2001).
[8] J. B. Bellicard, P. Bounin, R. F. Frosch, R. Hofstadter, J. S. McCarthy, F. J. Uhrhane, M. R. Yearian, B. C. Clark, R. Herman, and D. G. Ravenhall, Phys. Rev. Lett. **19**, 527 (1967).
[9] H. J. Emrich *et al.*, Nucl. Phys. A **396**, 401c (1983).

[10] E. Caurier *et al.*, Phys. Lett. B **522**, 240 (2001), and references therein.
[11] G. Fricke *et al.*, At. Data Nucl. Data Tables **60**, 177 (1995), and references therein.
[12] A. M. Stefanini *et al.*, Phys. Lett. B **679**, 95 (2009).
[13] H. A. Aljuwair *et al.*, Phys. Rev. C **30**, 1223 (1984).
[14] G. Montagnoli *et al.*, Phys. Rev. C **85**, 024607 (2012).
[15] C. L. Jiang, B. B. Back, H. Esbensen, R. V. F. Janssens, and K. E. Rehm, Phys. Rev. C **73**, 014613 (2006).
[16] M. Dasgupta, D. J. Hinde, A. Diaz-Torres, B. Bouriquet, C. I. Low, G. J. Milburn, and J. O. Newton, Phys. Rev. Lett. **99**, 192701 (2007).
[17] C. Mahaux, H. Ngô, and G. R. Satchler, Nucl. Phys. A **449**, 354 (1986).
[18] E. Crema *et al.*, Phys. Rev. C **84**, 024601 (2011).
[19] J. F. P. Huiza, E. Crema, A. Barioni, D. S. Monteiro, J. M. B. Shorto, R. F. Simões, and P. R. S. Gomes, Phys. Rev. C **82**, 054603 (2010).
[20] H. Timmers *et al.*, Nucl. Phys. A **584**, 190 (1995); **633**, 421 (1998).
[21] N. Rowley *et al.*, Phys. Lett. B **373**, 23 (1996).
[22] V. I. Zagrebaev, Phys. Rev. C **78**, 047602 (2008).
[23] K. E. Rehm *et al.*, Phys. Rev. C **37**, 2629 (1988).
[24] S. Mitsuoka, H. Ikezoe, K. Nishio, K. Tsuruta, S. C. Jeong, and Y. Watanabe, Phys. Rev. Lett. **99**, 182701 (2007).
[25] L. Corradi, G. Pollarolo, and S. Szilner, J. Phys. G **36**, 113101 (2009).
[26] M. Evers, M. Dasgupta, D. J. Hinde, L. R. Gasques, M. L. Brown, R. Rafiei, and R. G. Thomas, Phys. Rev. C **78**, 034614 (2008).
[27] M. Evers, M. Dasgupta, D. J. Hinde, D. H. Luong, R. Rafiei, R. du Rietz, and C. Simenel, Phys. Rev. C **84**, 054614 (2011).
[28] C. J. Lin *et al.*, Phys. Rev. C **79**, 064603 (2009).
[29] S. Yusa, K. Hagino, and N. Rowley, Phys. Rev. C **85**, 054601 (2012).
[30] D. S. Monteiro *et al.*, Phys. Rev. C **79**, 014601 (2009).
[31] L. C. Chamon *et al.*, Phys. Rev. C **66**, 014610 (2002).
[32] I. J. Thompson, Comp. Phys. Rep. **7**, 167 (1988).
[33] Evaluated Nuclear Structure Data Files, National Nuclear Data Center, Brookhaven National Laboratory [http://www.nndc.bnl.gov].
[34] N. Takigawa, K. Hagino, M. Abe, and A. B. Balantekin, Phys. Rev. C **49**, 2630 (1994).
[35] K. Hagino, N. Takigawa, M. Dasgupta, D. J. Hinde, and J. R. Leigh, Phys. Rev. Lett. **79**, 2014 (1997).
[36] S. Sinha, M. R. Pahlavani, R. Varma, R. K. Choudhury, B. K. Nayak, and A. Saxena, Phys. Rev. C **64**, 024607 (2001).
[37] H. Esbensen, C. L. Jiang, and A. M. Stefanini, Phys. Rev. C **82**, 054621 (2010).